USNA---Trident Scholar project report; no. 327 (2004)

The Effect of Surface Roughness on Hydrodynamic Drag and Turbulence

By

Midshipman 1/C Thomas A. Shapiro, Class of 2004
United States Naval Academy
Annapolis, Maryland

_____
(Signature)

_____
(Date)

Certification of Advisers Approval

Assistant Professor Michael P. Schultz
Naval Architecture and Ocean Engineering Department

_____
(Signature)

_____
(Date)

Associate Professor Karen A. Flack
Mechanical Engineering Department

_____
(Signature)

_____
(Date)

Acceptance for the Trident Scholar Committee

Professor Joyce E. Shade
Deputy Director of Research & Scholarship

_____
(Signature)

_____
(Date)

REPORT DOCUMENTATION PAGE

Form Approved
OMB No. 074-0188

1. AGENCY USE ONLY (Leave blank)	2. REPORT DATE	3. REPORT TYPE AND DATE COVERED
	5 May 2004	

4. TITLE AND SUBTITLE
The effect of surface roughness on hydrodynamic drag and turbulence

5. FUNDING NUMBERS

6. AUTHOR(S)
Shapiro, Thomas A. (Thomas Alan), 1982-

7. PERFORMING ORGANIZATION NAME(S) AND ADDRESS(ES)		8. PERFORMING ORGANIZATION REPORT NUMBER

9. SPONSORING/MONITORING AGENCY NAME(S) AND ADDRESS(ES)		10. SPONSORING/MONITORING AGENCY REPORT NUMBER
US Naval Academy Annapolis, MD 21402		Trident Scholar project report no. 327 (2004)

11. SUPPLEMENTARY NOTES

12a. DISTRIBUTION/AVAILABILITY STATEMENT	12b. DISTRIBUTION CODE
This document has been approved for public release; its distribution is UNLIMITED.	

13. ABSTRACT: The ability to accurately predict the drag forces on a ship before it is built would lead to more efficient designs. To do this, the effect of surface roughness on frictional drag must be well understood. The goal of this project is to identify the appropriate roughness scaling parameters for simple three-dimensional roughness with similar length scales to those found on ship hulls. In order to study and ultimately predict the effects of surface roughness on fluid flow and drag, flat plates with smooth and rough surface conditions were tested. Mesh and sandpaper were chosen as the rough surfaces because they are three dimensional, which is characteristic of naturally occurring surfaces. The first phase of testing involved towing the plates in a tow tank to determine the overall frictional drag. These tests were done in the 115 m long tow tank located in the USNA Hydromechanics Laboratory. Detailed velocity measurements were also obtained with the plates in a re-circulating water channel located in the Hydromechanics Laboratory to determine the effect of the roughness on the turbulence near the surface. The velocity measurements were obtained with a laser Doppler velocimeter (LDV). The drag results from both sets of tests showed excellent agreement. It was also observed that beyond a few roughness heights from the wall, the normalized turbulence was independent of the roughness. Proper scaling for the sandpaper was found to be a function of the roughness height, while the mesh surfaces were discovered to be a function of both roughness height and wire spacing. The results from this project will aid in the development of a general model of overall frictional drag from physical measures of the surface alone.
.
.

14. SUBJECT TERMS: boundary layer; skin-friction drag; surface roughness; turbulence; resistance	15. NUMBER OF PAGES 58
	16. PRICE CODE

17. SECURITY CLASSIFICATION OF REPORT	18. SECURITY CLASSIFICATION OF THIS PAGE	19. SECURITY CLASSIFICATION OF ABSTRACT	20. LIMITATION OF ABSTRACT

Abstract

The ability to accurately predict the drag forces on a ship before it is built would lead to more efficient designs. To do this, the effect of surface roughness on frictional drag must be well understood. The goal of this project is to identify the appropriate roughness scaling parameters for simple three-dimensional roughness with similar length scales to those found on ship hulls. In order to study and ultimately predict the effects of surface roughness on fluid flow and drag, flat plates with smooth and rough surface conditions were tested. Mesh and sandpaper were chosen as the rough surfaces because they are three dimensional, which is characteristic of naturally occurring surfaces. The first phase of testing involved towing the plates in a tow tank to determine the overall frictional drag. These tests were done in the 115 m long tow tank located in the USNA Hydromechanics Laboratory. Detailed velocity measurements were also obtained with the plates in a re-circulating water channel located in the Hydromechanics Laboratory to determine the effect of the roughness on the turbulence near the surface. The velocity measurements were obtained with a laser Doppler velocimeter (LDV). The drag results from both sets of tests showed excellent agreement. It was also observed that beyond a few roughness heights from the wall, the normalized turbulence was independent of the roughness. Proper scaling for the sandpaper was found to be a function of the roughness height, while the mesh surfaces were discovered to be a function of both roughness height and wire spacing. The results from this project will aid in the development of a general model of overall frictional drag from physical measures of the surface alone.

Acknowledgements

I would like to thank the staff of the Hydromechanics Laboratory located at the United States Naval Academy for all of there support. Without their expertise and equipment this project would never have been possible. I would also like to thank Professor Shade and the rest of the Trident Scholar Committee for all the time they spent reviewing the projects. Finally, I would like to thank my advisors for this project, Professor Schultz and Professor Flack for giving up countless hours helping me with this project. Without their guidance and expertise this project would have been impossible.

TABLE OF CONTENTS

List of Figures

List of Tables

1. Nomenclature

C_f Coefficient of skin friction $= \dfrac{\tau_w}{\frac{1}{2}\rho U^2}$

C_F Coefficient of frictional drag, $Drag = \dfrac{F_D}{\frac{1}{2}\rho U^2 S}$

$C_{Fsmooth}$ Coefficient of frictional drag for a smooth surface

C_{Frough} Coefficient of frictional drag for a rough surface

C_A Correlation allowance

C_T Total resistance coefficient

d Centerline mesh wire spacing

F_D Force of drag

F_{raw} Force measured by force gauges

F_{tare} Wave-making forces

k Roughness length scale

k^+ Roughness Reynolds number

L Length of plate

L^+ Ratio of length of plate to viscous length scale

p Mesh wire diameter

Re_L Reynolds number, $\mathrm{Re}_L = \dfrac{\rho U L}{\mu}$

R_t Maximum peak to trough roughness height

R^2 The coefficient of determination

S	Wetted surface area of plate
U	Mean axial velocity
U_e	Free stream velocity
U_τ	Friction velocity $U_\tau = \sqrt{\frac{\tau_w}{\rho}}$
ΔU^+	Roughness function
$\Delta U^{+'}$	Slope of the roughness function
u'^{2+}	Axial Reynolds normal stress
v'^{2+}	Wall-normal Reynolds normal stress
$-u'v'^{+}$	Reynolds shear stress
y	initial distance from the wall including wall datum offset
y_{raw}	initial distance from the wall
δ	Boundary layer thickness, y location where $U=0.995U_e$
δ^*	Displacement thickness, $\delta^* = \int_0^\infty \left(1 - \frac{U}{U_e}\right) dy$
ε	Wall datum offset
κ	von Karman constant
μ	Absolute viscosity of fluid
ρ	Density of fluid
θ	Momentum thickness, $\theta = \int_0^\infty \left(1 - \frac{U}{U_e}\right)\frac{U}{U_e} dy$
τ_w	Wall shear stress
ν	Kinematic viscosity if fluid

2. Introduction

Being able to accurately predict the force of drag on a ship or an airplane before it is built would greatly aid in the design. The United States Navy would benefit greatly from this ability. Predicting the drag forces on a ship before it is built would allow for them to be designed to sail faster, longer, and more efficiently. Furthermore, understanding and predicting the effects of drag would help in the development and performance of turbines, compressors and other bladed turbomachines whose characteristics are changed and affected by surface roughness(Acharya, Bornstein, and Escudier 1986).

When designing ships, one method of predicting drag involves model testing. The laws of similitude allow for the behavior of full scale prototypes to be predicted from models. For model ships, it is important that the model and prototype have the same shape and differ only in size. One problem is that the size of the surface roughness is very hard to reduce proportionally to the reduced size of the ship (Franzini 1997). Hence, it is impossible to predict how much of the drag is actually caused by the surface roughness. In order to compensate for this, engineers add a correlation allowance, C_A, to the total resistance coefficient, C_T, to get a drag coefficient which accommodates surface roughness (Lewis 1988). The allowance coefficient is completely empirical, representing an average roughness condition. Further work was done specifically in hull roughness effects which related a roughness height to C_A (Bowden & Davison 1974). The problem with this method is that the effective roughness height still needs to be found experimentally. An improved resistance coefficient would relate surface frictional drag to a specific, measured surface roughness. This knowledge would greatly aid ship designers.

The purpose of this research project was to examine the effects that two different surface roughness types have on drag. From the results, a model which correlates these particular

surface roughnesses to their associated drag can be created. The model results could then be scaled up to ship scale to see how the surface roughness increases the overall drag and required propulsion power of a ship.

3. Background

Drag is defined as the net force in the direction of the flow opposing the motion of the body through a fluid (Alexandrou 2001). For a ship, drag is comprised of two main components, wave-making drag and viscous drag, which can be added together to get the total drag force. When ships move through water, waves are created. These waves are created by the varying pressure that the ship is causing under the water and the constant pressure at the surface (Tupper 1996). The energy needed to make these waves is provided by the ship. Viscous drag is comprised of both pressure drag and friction drag. Pressure drag is the drag produced by normal stresses on the surface of the body. A plate perpendicular to the flow has nearly all pressure drag which is caused by the difference in pressure between the flow on the upstream and downstream side of the plate (Munson, Young, and Okiishi 2002). For a plate parallel to the flow, the pressure drag is minimal, and the drag is mainly due to friction. Friction drag is created by shear stresses, which are caused by viscous and turbulent effects. With turbulent flows, which include most flows of practical interest, surface roughness can significantly increase the frictional drag force (Munson, Young, and Okiishi 2002).

Numerous research studies (Schoenherr 1932, Granville 1987, and Grigson 1987, 1992) have been conducted regarding how surface roughness affects a ship's drag. These studies focus on ways to scale tow test data of models covered with a surface roughness up to that of full scale ships in order to determine the actual drag associated with surface roughness. Because model tests alone will not give the full scale viscous drag on a ship, these studies have focused on measuring the associated roughness function which can then be used to get the full scale viscous drag on a ship (Grigson 1987). Other methods for predicting the behavior of flids on surfaces

involve using Computational Fluid Dynamics (CFD) to perform Direct Numerical Simulation (DNS). The problem with DNS in the present case is that computing turbulent flows requires a very large computational grid at high Reynolds numbers. There are two main length scales that DNS have to account for: the viscous length scale which is of the order of microns, and the boundary layer length scale which is of the order of centimeters. The DNS must capture the flow physics at the viscous length scale throughout the entire boundary layer. At present, computers are not able to perform the large number computations in a reasonable time. Some CFD codes using turbulence models using a simplified computational grid including numerous assumptions have been developed which includes surface roughness effects. Furthermore, results from experiments are still needed as inputs to the models.

As fluid flows over a surface, a thin layer develops right above the surface due to viscosity. In this thin layer, called the boundary layer, the velocity of the flow varies from zero at the wall to the flow speed at the edge of the layer. An example of a turbulent boundary layer mean velocity profile can be seen in Figure 1. Many things affect this thin boundary layer, including the type of flow (laminar or turbulent), the speed of the flow, and fluid properties. With turbulent flows, surface roughness affects the boundary layer near the wall by creating higher wall shear stress. This in turn creates more frictional drag.

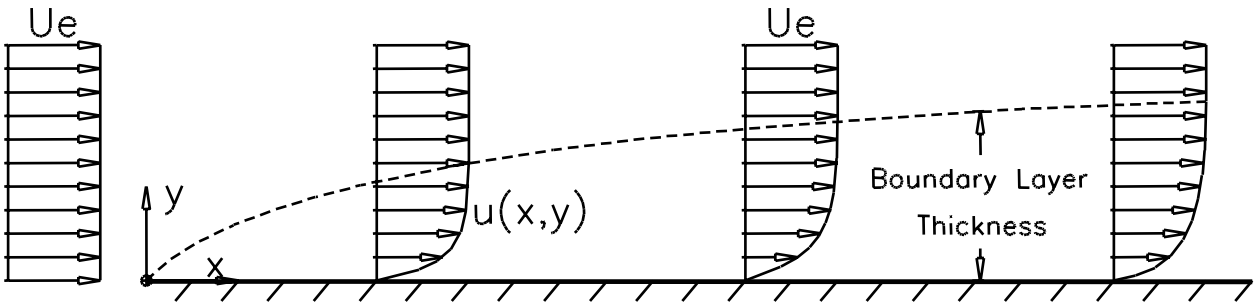

(a)

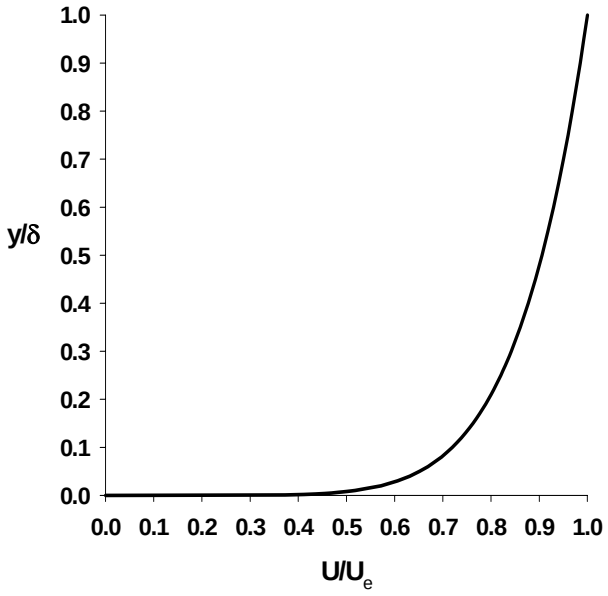

(b)

Figure 1–Turbulent boundary layer velocity profile: (a) boundary layer development; (b) non-dimensional profile

A turbulent boundary layer can be modeled as a composite of various layers, as shown in Figure 2. The first layer adjacent to the wall, which is known as the viscous sublayer, has shear stress caused almost entirely by viscosity. Viscosity is a fluid's internal resistance to shear deformation (Alexandrou 2001). This sublayer is extremely thin, generally extending only a few

hundredths of a millimeter out from the wall (Franzini 1997). The outer layer is the region in which viscosity does not have a direct effect on shear stress. Instead, the shear stress in this outer layer region is caused by turbulent motions. Between the sublayer and outer layer, the log-law region is the location where the total shear stress is nominally constant and maximum. Turbulent stresses also dominate in this region. The log region is characterized by the linear velocity profile when plotted in log-normal coordinates (Clauser 1954).

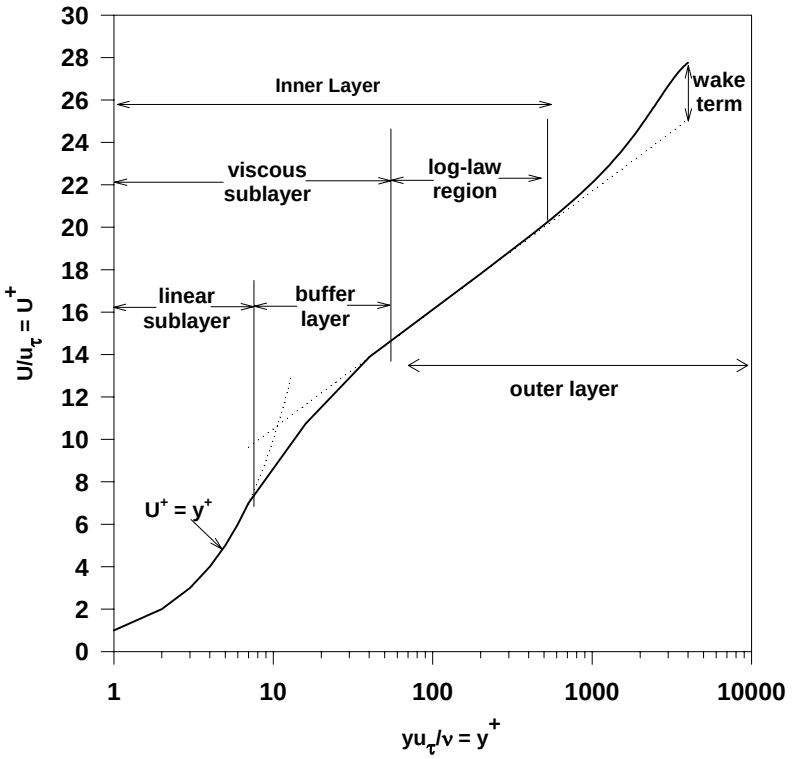

Figure 2-The mean velocity profile for a smooth-wall turbulent boundary layer

Typically, a boundary layer over a rough surface is modeled by the same methods as a smooth wall boundary layer. This model uses a standard two-layer approach in which only the inner layer is directly affected by the roughness, while the outer layer is affected only indirectly through the increase in the wall shear stress. The effects of surface roughness close to the wall

are not well understood (Acharya, Bornstein, and Escudier 1986). Further research is needed in this area.

Surface roughness is thought to affect the mean velocity profile by shifting it downward when plotted in log-normal coordinates. The drag associated with the roughness decreases the momentum of the flow. This loss of momentum can be seen in the Figure 3 where ΔU^+, the roughness function, represents the effect of roughness on the mean velocity profile. The larger the roughness function is, the more effect the roughness has on the mean profile and hence the wall shear stress (Hama 1954). This increase in wall shear stress will in turn create more drag. Another important feature to note is how the rough surface profile maintains the same shape as the smooth wall profile. If the surface roughness were to affect the outer layer, the mean velocity profile for the rough surface in the outer layer would not have the same shape as the smooth wall. Since the current two layer model of the traditional boundary layer assumes that the outer layer is not affected by surface roughness, modifications of the current model would need to be made.

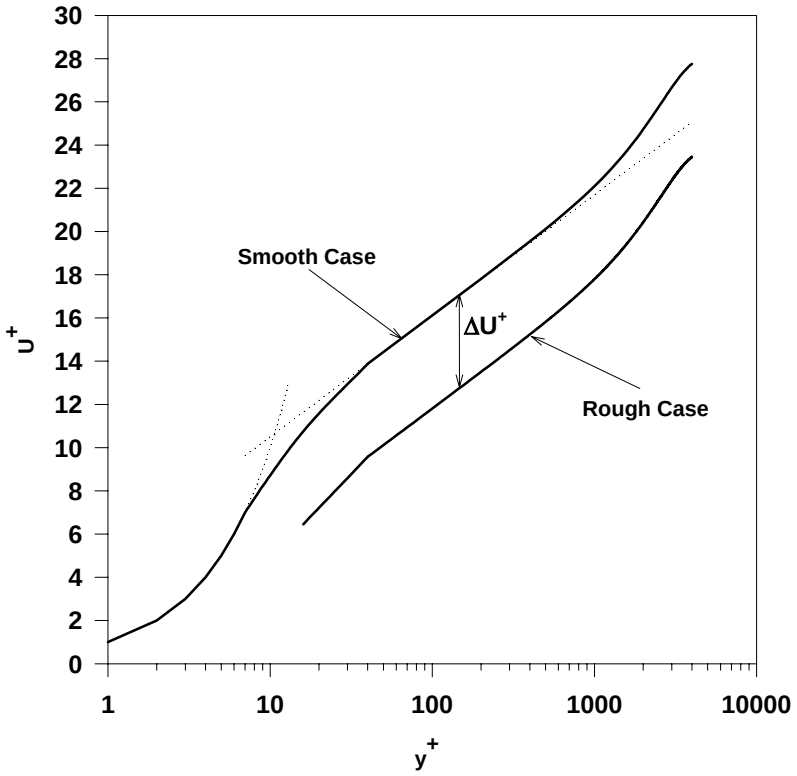

Figure 3-Turbulent boundary layer profiles: smooth and rough wall

The effects of surface roughness on mean velocity profiles have been the topic of many research studies. This can be seen in the works of Clauser (1954), Hama (1954), Granville (1987), and Schultz and Myers (2003). Much of this work was done in order to determine the roughness function and to show that increasing the surface roughness merely increases the downward shift of the mean velocity profile. For these studies, the roughness function, ΔU^+, was obtained by measuring the mean velocity profile directly or by using a tow tank and backing out the roughness function via boundary layer similarity models.

Previous research has shown that at sufficiently high Reynolds number, surface roughness does not affect the turbulent flow outside a sublayer that extends a few roughness heights above the surface (Rotta 1962, Townsend 1976). This implies that very little

communication occurs between the near-wall region and the rest of the flow. Recent papers, however, claim that the effects of surface roughness are not confined to the wall region (Antonia and Krogstad 2001), but can extend beyond the log law region. Additionally, they claim that surface roughness affects the turbulent stresses that contribute to surface drag. However, there is not a general consensus regarding the extent and influence of surface roughness on turbulence among researchers in the field. (Krogstad and Antonia 1999).

Because the traditional two layer model of the turbulent boundary layer has recently been called into question, new research must be done in order to explain the conflicting findings which have been seen by some engineers. Some of the recent findings may have been a result of using different surface roughness geometries which affected the boundary layer in a unique way that is not characteristic of other types of surface roughness. Furthermore, there must be some roughness height at which current boundary layer models fail because the surface roughness becomes too large for its effects on the flow structure to be confined to the inner layer. This information would be very helpful in predictions of drag for ships.

The goal of this project was to experimentally investigate these questions. The drag on three types of surfaces was obtained. A smooth plate was used as a control surface. Mesh surfaces along with sandpaper surfaces, three of each, were tested as the rough surfaces. Mesh and sandpaper were chosen as the rough surfaces because they are three dimensional, which is characteristic of naturally occurring surfaces, they are easily repeatable, and there is some data already available in literature for these surfaces. The height of the roughness elements for the mesh and sandpaper were varied to determine if typical boundary layer models are valid for large roughness heights. The first phase of testing involved towing the plates in a tow tank to determine the frictional drag on the plate. These tests were done in the 115 m long tow tank

located in the USNA Hydrodynamics Laboratory. Next, detailed velocity measurements were obtained with the plates in a re-circulating water channel located in the hydrodynamics lab to determine the effect of the roughness on the turbulence near the surface, by measuring mean and turbulent velocities in the boundary layer. These detailed velocity measurements were obtained with a laser Doppler velocimeter (LDV).

4. Experimental Procedures-Tow Tank Tests

All drag measurements made on the plates were done in the 115 meter tow tank located in the Hydromechanics Laboratory located at the United States Naval Academy. The width and depth of the tank are 7.9 and 4.9 meters, respectively. The towing carriage, which is powered by two 300 kW motors, can vary its velocity between 0 and 7.62 m/sec. With this research project, the speed range was 1.8 and 3.7 m/s. The plates were 1.52 meters long and 0.56 meters wide, with a thickness of 3.8 mm. They were covered on both sides with the given surfaces which were held on using epoxy. The plates were then secured to the towing carriage using the apparatus shown in Figure 4.

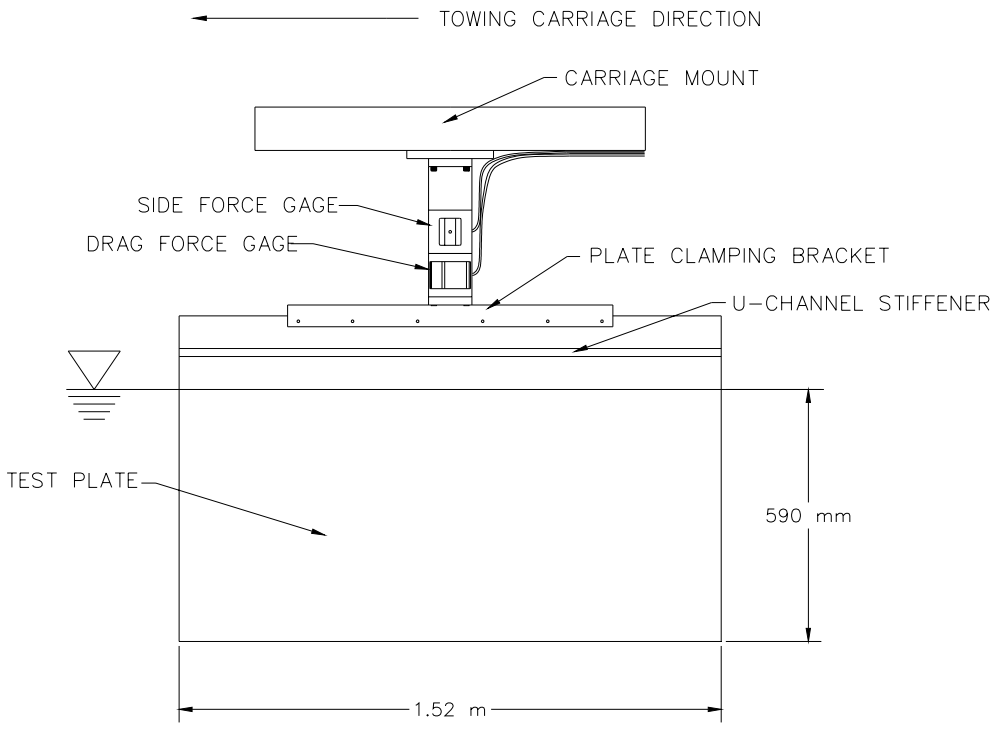

Figure 4-Schematic of the flat plate drag apparatus for towing tank tests

A stiffener was put on the top of the plates so that the plate would not bend when being towed through the water. Two force gages were then attached to the plate. The first gage measured the force parallel to the plate which was the actual viscous drag force. The second gage measured the forces acting perpendicular to the plate which were the side forces. These forces are not important to the drag calculations; however, attempts were made to minimize the side forces to ensure the plate was parallel to the flow. This was done by towing a plate several times while monitoring the side forces, and then making adjustments on the alignment of the plate.

The force gages start off as a solid block of magnetic stainless steel. They are then hollowed out in such a way so that they only deflect in one direction when a force is applied. A displacement transducer is then used to measure the distance the gage deflects. The transducer has a fixed coil and a ferrous core that is free to move in the direction of the displacement. A signal conditioning unit, (SCU), sends a high frequency AC current to the coil. As the gage is displaced by a force, the ferrous core moves inside the coil and changes the AC current. This signal is then sent back to the SCU where it is converted to a DC voltage. This voltage is now proportional to the displacement of the gage.

Before setting the gages on the plate, they have to be calibrated to determine what DC voltage is output when known forces deflect the gages. This is done by hanging weights off the gages and recording the voltage of the SCU. Using this information, a linear calibration plot can be made that relates force and voltage. The slope of this plot is used to convert the force gage output voltages into force measurements. An example of the calibration plot can be seen in Figure 5.

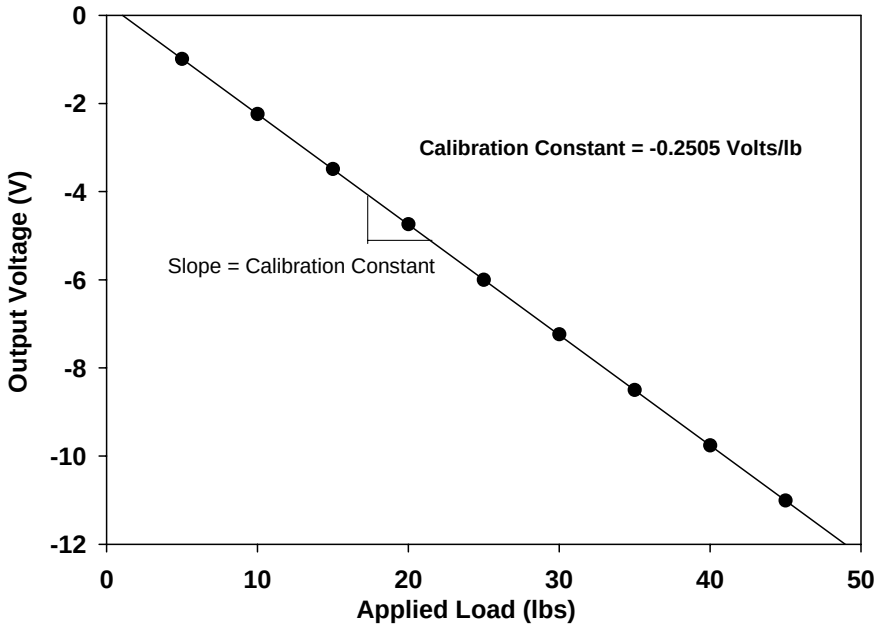

Figure 5-Force gage calibration curve

The analog signal from the SCU is then sent to an analog to digital, A to D, converter. After going through the A to D converter, the signal is then sent to a computer for data acquisition. The voltage from the SCU is multiplied by the calibration constant gotten from the calibration plot to determine the measured drag force. A block diagram of the different parts of this process is shown in Figure 6.

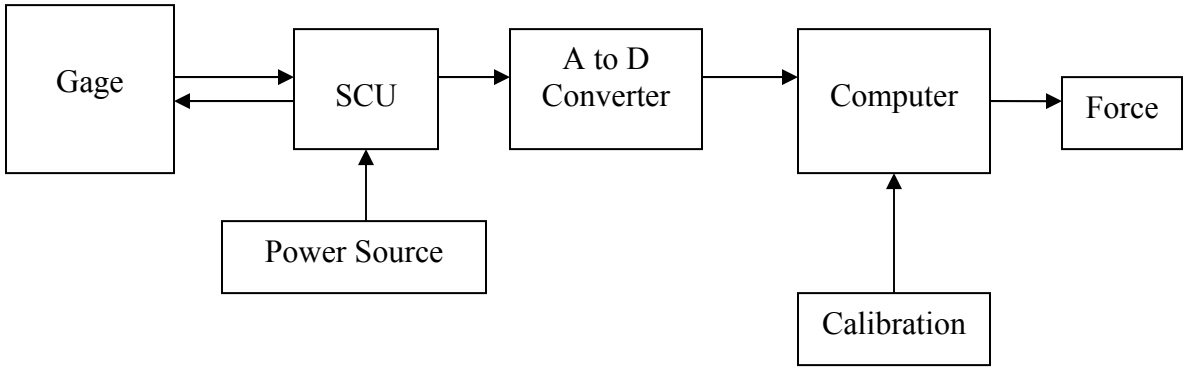

Figure 6-Block diagram for force measurements

5. Experimental Analysis of the Tow Tank Results

One smooth plate and six plates with different roughness (three sandpaper and three mesh) were tested. The drag force for each surface roughness was measured. Initially the wave making forces associated with the towed plates were measured. This was done by towing a smooth plate with 2.54 cm of it submerged in the water. The force measured was then assumed to be caused primarily by wave-making forces although, the frictional forces were accounted for in the final equation by subtracting this wetted surface area from the total wetted surface area. The plates were then submerged 56 cm below the water surface. In previous research (Schultz, private communication), wave profiles were observed, photographed, and analyzed for plates that were fully submerged and for plates that were partially submerged 2.54 cm. It was concluded from these tests that for a flat plate, waves were caused by surface piercing rather than by how much of the plate was below the water line. When towed at seven different speeds, force measurements, which were called the raw forces, were recorded by the force gauges on the plate. The previously measured wave-making forces, called tare forces, F_{tare}, were then subtracted from the measured raw forces, F_{raw}. The result is the frictional drag force, F_D, on the plate, as demonstrated in equation 1.

$$F_D = F_{raw} - F_{tare} \tag{1}$$

By knowing the velocity that the plates were towed at and the drag forces that were measured, the coefficient of frictional drag, C_F, can be calculated. This is done by dividing the drag force by the dynamic pressure, $(\frac{1}{2}\rho U^2)$ where ρ is the density of the fluid and U is the towing velocity, and the wetted surface area of the plate, S. This can be seen in equation 2.

$$C_F = \frac{F_D}{\frac{1}{2}\rho U^2 S} \tag{2}$$

For a smooth wall, C_F is a function of the Reynolds number, Re_L. The Reynolds number is a non-dimensional number which represents the ratio of inertial forces to viscous forces, and as the Reynolds number increases beyond the critical value for transition, turbulence increases (Franzini 1997). The Reynolds number is expressed in equation 3

$$\mathrm{Re}_L = \frac{\rho UL}{\mu} \tag{3}$$

where L is the length of the plate and μ is the dynamic viscosity of the fluid.

For the smooth wall, the coefficient of frictional drag decreases with increasing Reynolds number. The reason for this is that both viscous and inertia forces are still present, but viscous forces are decreasing. For a fully rough wall, C_F is independent of the Reynolds number at high Reynolds numbers because turbulent stresses dominate the viscous stresses, as illustrated in Figure 7.

When C_F is known, Granville's Similarity Theory can be used to calculate the roughness function, ΔU^+ (Granville 1987). The roughness function is a crucial value because it allows for drag to be scaled up to larger objects. Granville's theory states that, for the same value of $Re_L C_F$, the difference between $\sqrt{\frac{2}{C_F}}$ of the smooth wall and $\sqrt{\frac{2}{C_F}}$ of the rough wall approximately equals the roughness function, ΔU^+ when plotted against $\log(Re_L C_F)$. Similarity theory states

that this calculation yields the same result as measuring the downward shift in the mean velocity profile at the trailing edge of the towed plate. An example of this is shown in Figure 8.

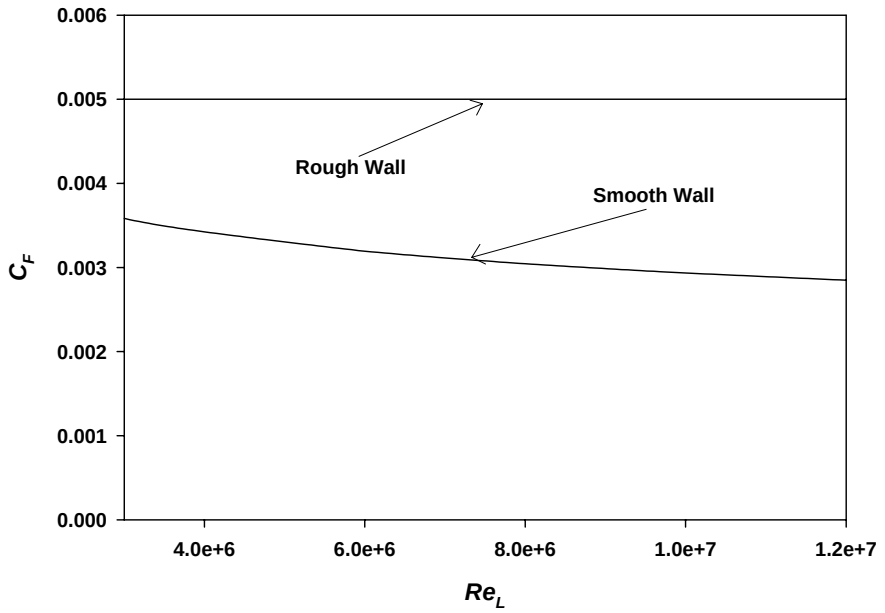

Figure 7-Coefficient of frictional drag: smooth and rough walls

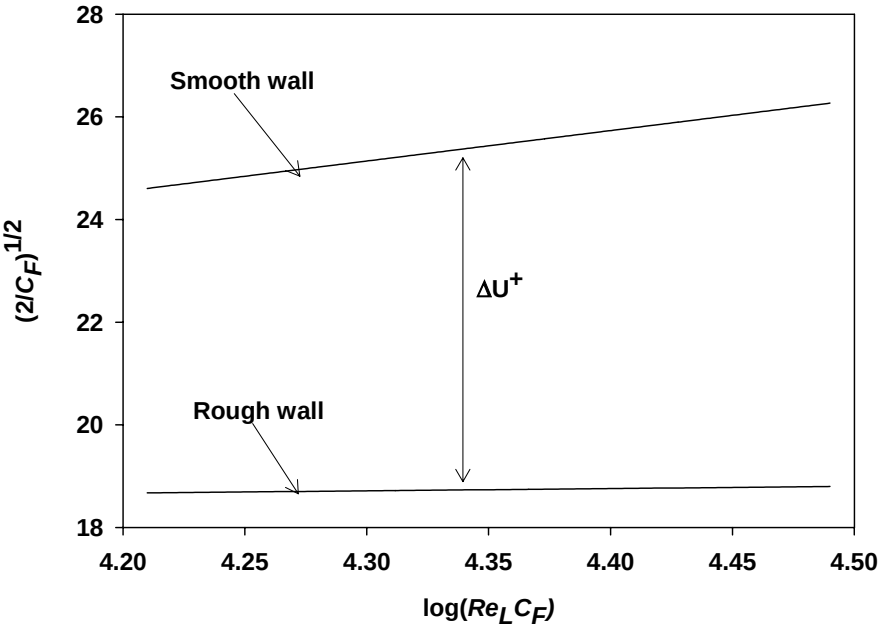

Figure 8-Relationship between ΔU^+ and coefficient of frictional drag

The Karman Schoenherr line which agrees closely (within 1%) with the present smooth wall results is used to get $\sqrt{\frac{2}{C_F}}$ of the smooth wall (Schoenherr 1932. The Karman Schoenherr line is given in equation 4.

$$\frac{0.242}{\sqrt{C_F}} = \log(\mathrm{Re}_L\, C_F) \tag{4}$$

Once $\sqrt{\frac{2}{C_F}}$ of the smooth wall is known, the roughness function for the towed plate data can be found. This is shown in equation 5.

$$\Delta U^+ = \left(\sqrt{\frac{2}{C_F}}\right)_S - \left(\sqrt{\frac{2}{C_F}}\right)_R - 19.7\left[\left(\sqrt{\frac{C_F}{2}}\right)_S - \left(\sqrt{\frac{C_F}{2}}\right)_R\right] - \frac{1}{\kappa}\Delta U^{+'}\left(\sqrt{\frac{C_F}{2}}\right)_R \tag{5}$$

Equation 5 shows Granville's similarity law where κ is the von Karman constant, which is equal to 0.41, and $\Delta U^{+'}$ is the roughness function slope. The roughness function slope is the slope of ΔU^+ as a function of $\ln(k^+)$. The roughness Reynolds number, k^+, is the ratio of the roughness length scale, k, to the viscous length scale, ν/U_τ. The roughness function slope is also needed in order to obtain k^+. This can be seen in equation 6 which is also a part of Granville's similarity law.

$$k^+ = \left(\frac{k}{L}\right)\left(\frac{R_{eL}C_F}{2}\right)\left(\sqrt{\frac{2}{C_F}}\right)_R\left[1-\frac{1}{\kappa}\left(\sqrt{\frac{C_F}{2}}\right)_R+\frac{1}{\kappa}\left(\frac{3}{2\kappa}-\Delta U^{+'}\right)\left(\frac{C_F}{2}\right)_R\right] \quad (6)$$

An iterative solution is required to solve for equations (5) and (6) since $\Delta U^{+'}$ is unknown in both cases. To begin with, $\Delta U^{+'}$ is taken to equal zero and the equations are solved and ΔU^{+} is plotted versus ln(k^+). The slope of this line is found, which can then be substituted back in for $\Delta U^{+'}$. This process is repeated until the slope of the line and $\Delta U^{+'}$ used in the equations converge.

Since it is impossible to determine the effect that surface roughness has on a ship through model tow tests, ΔU^{+} is found by towing flat plates which can then be scaled up to determine what C_F is for full scale ships. This is done by using Granville's similarity law for scaling up C_F (Schultz 1998). Initially, the smooth coefficient of friction, $C_{Fsmooth}$, is determined for a ship using equation (4). $C_{Fsmooth}$ is then plotted against log (Re_L). A new curve representing C_{Frough} is created by shifting the $C_{Fsmooth}$ curve by a distance of $\Delta U^{+}/(\ln(10)/\kappa)$ in the positive log(Re_L) direction (Schultz 1998). This can be seen in Figure 9. The location of the experiment value of C_{Frough} from the tow tank tests on the displaced curve is also shown on Figure 9. As expected, this value falls on the C_{Frough} curve.

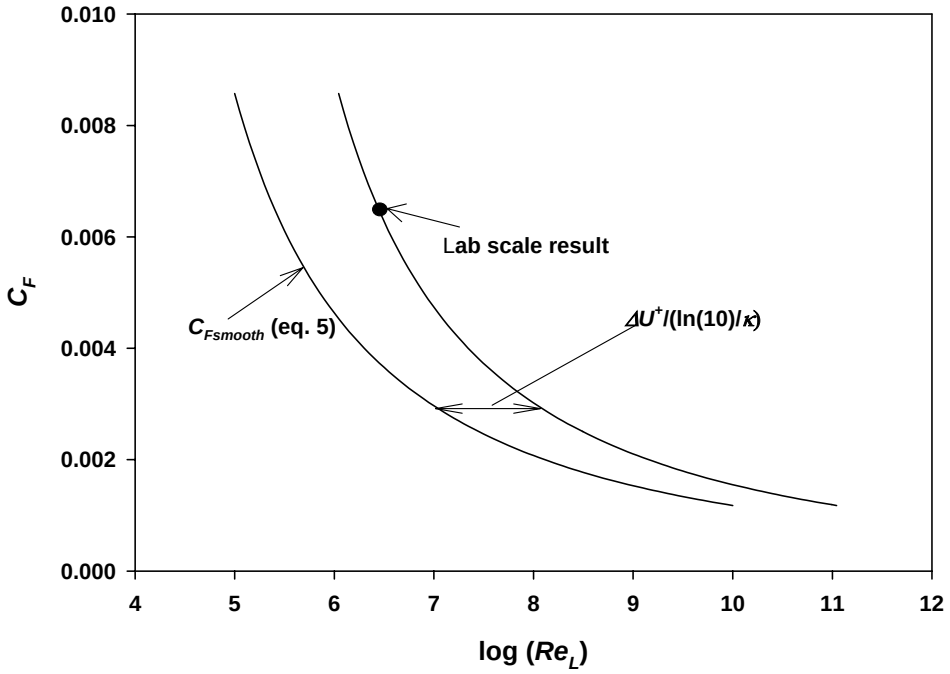

Figure 9-$C_{Fsmooth}$ and experimental C_F

The ratio of the plots length to the viscous length scale is called L^+. A line of constant L^+ passing through the lab scale data is created using equation 7.

$$L^+ = \mathrm{Re}_L\left(\sqrt{\frac{C_F}{2}}\left(1-\frac{1}{\kappa}\sqrt{\frac{C_F}{2}}\right)\right) \tag{7}$$

This can be seen in Figure 10.

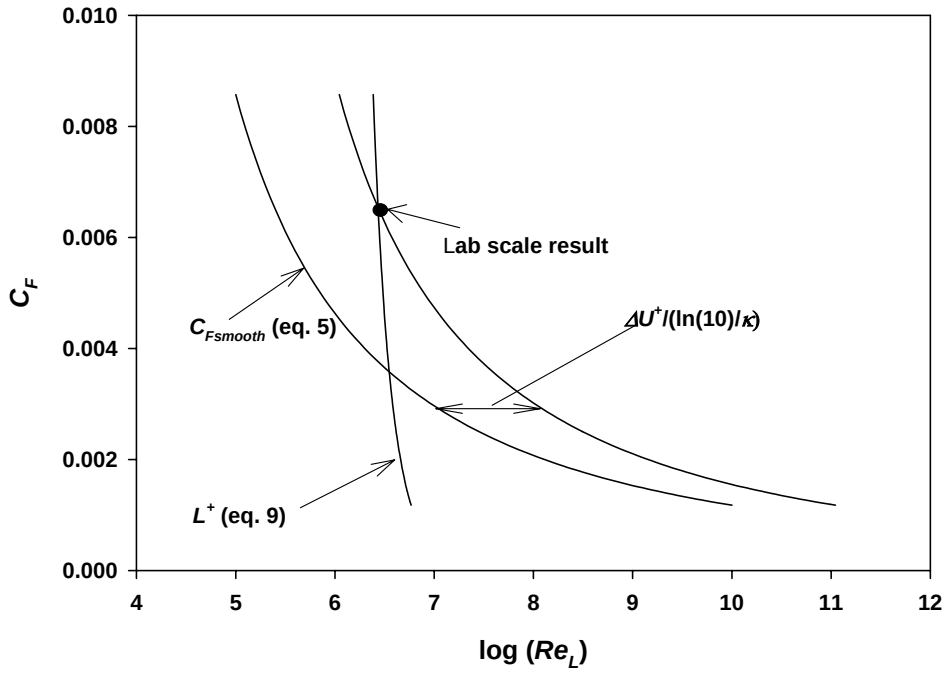

Figure 10-Line of constant L^+

This line of constant L^+ is then shifted in the positive log (Re_L) direction by a distance of log($L_{ship\ scale}/L_{lab\ scale}$) (Schultz 1998). The intersection of the shifted L^+ line and the C_{Frough} line gives the scaled up result of C_{Frough} for a full scale ship. This can be seen in Figure 11.

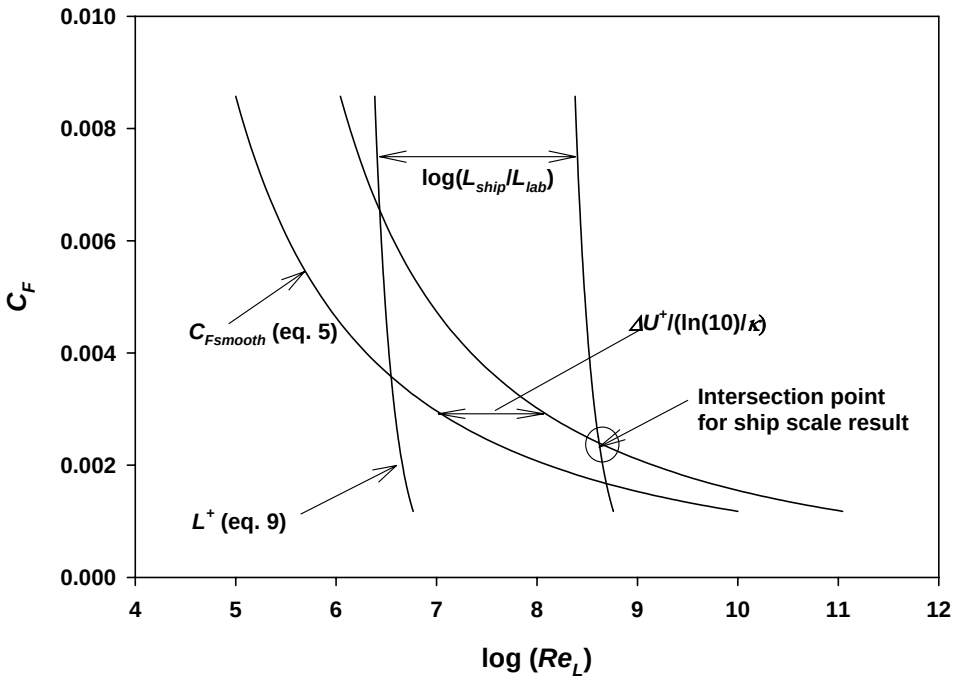

Figure 11-Schematic of Granville scale-up procedure

Furthermore, the Reynolds number where this intersection occurs can be recorded from Figure 11. Using the Reynolds number, the speed at which the full scale ship would be cruising at can be calculated. This is done using equation 8

$$U = \frac{\mathrm{Re}_L \nu}{L} \tag{8}$$

where U is the ship's speed and L is the length of the ship which was taken to be 150 meters.

This length is the same length as a DDG-51 destroyer, so this would be the speed that this destroyer was operating at. Next the $C_{Fsmooth}$ is determined for a full scale ship. This is done by using equation 5 and plugging the new Re_L values that were found for a full scale ship. With this

known, the percent increase in the coefficient of frictional drag due to roughness can be found using equation 9.

$$\frac{C_{Frough} - C_{Fsmooth}}{C_{Fsmooth}} = \% \text{ increase in frictional drag due to roughness} \quad (9)$$

Ships spend most of their time operating at or near their cruising speed. It is important to note how roughness affects the drag at this speed. For a DDG-51 class destroyer, this speed is around 15 knots. With this information, it is then possible to find how the percent increase in the coefficient of frictional drag due to roughness affects the total coefficient of drag. Using data already taken from model tests of a DDG-51, the coefficient of drag due to friction is found at certain speeds as well as the total drag coefficient. Using equation 10

$$\frac{C_F}{C_T} = \% \text{ of drag due to friction} \quad (10)$$

where C_F is the coefficient of drag due to friction and C_T is the coefficient of the total drag, the percent of drag due to friction can be found.

By multiplying the percent of drag due to friction and the percent increase in the coefficient of friction due to surface roughness, the percent increase in the total drag coefficient due to roughness can be found.

6. Discussion of Tow Tank Results

The frictional drag coefficient for the seven surfaces tested is shown on Figure 12. For fully rough surfaces, C_F is constant for the range of Reynolds numbers tested. The smooth surface shows a decrease in C_F with increasing Reynolds number. This graph shows that all of the surfaces tested are fully rough except for possibly the 80 grit sandpaper which shows a slight decrease in C_F with increasing Re_L. This does not affect our results in any way since Granville's similarity theory can be used for surfaces that do not fall in the fully rough regime.

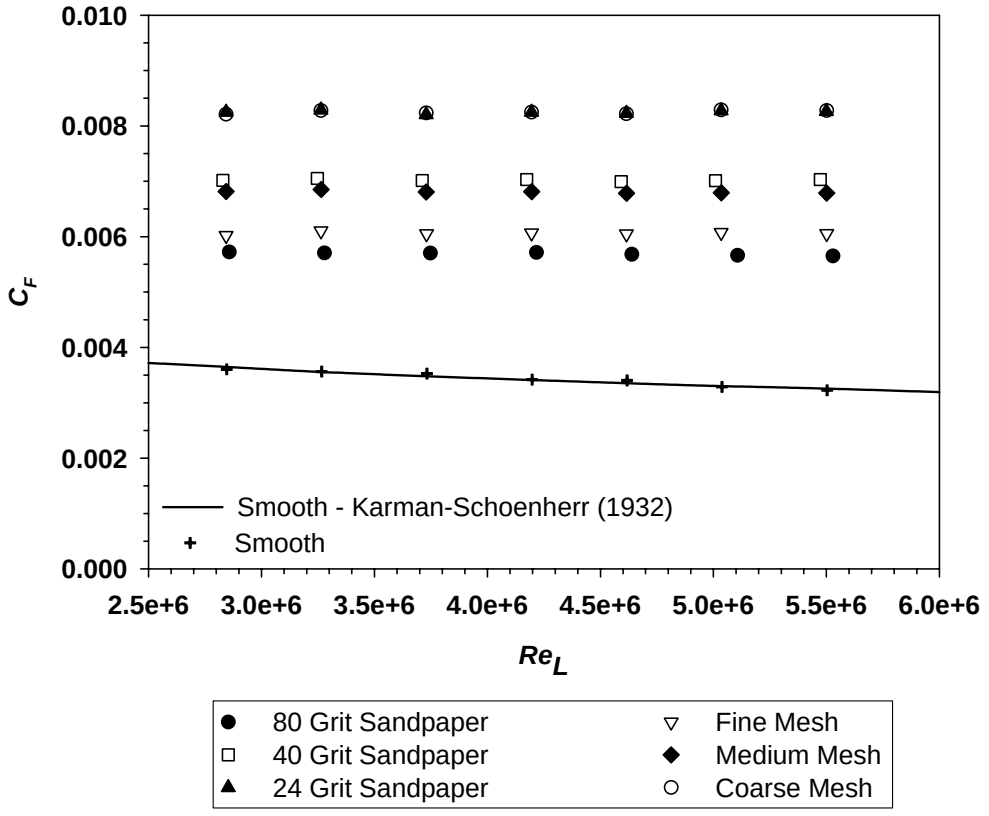

Figure 12-C_F vs. Re_L (Overall uncertainty at 95% confidence of C_F is 2%)

Using equation 5, the roughness functions for all the surfaces tested were calculated. As expected, the rougher a surface was, the larger its roughness function was. This means that the surface roughness with the larger roughness function should also have the highest drag. Table 1 shows the roughness functions for the present experimental matrix used in this investigation.

Table 1 – The roughness functions for the tow tank tests

	Roughness Functions (ΔU^+)					
Speed (m/s)	80 Grit	40 grit	24 Grit	Fine Mesh	Medium Mesh	Course Mesh
1.86	5.86	8.23	10.08	6.47	7.94	10.03
2.13	6.19	8.65	10.49	6.99	8.36	10.48
2.44	6.53	8.94	10.73	7.24	8.63	10.77
2.74	6.86	9.28	11.09	7.58	8.95	11.09
3.01	7.04	9.46	11.31	7.79	9.15	11.30
3.29	7.25	9.72	11.60	8.07	9.39	11.62
3.59	7.43	9.98	11.82	8.26	9.61	11.84

Using equations (5) and (6), the roughness function ΔU^+ and the roughness Reynolds number, k^+, were found for the mesh and sandpaper surfaces. This enables the full scale C_{Frough} to be determined as shown in Figure 11. For a DDG-51 at 15 knots, 65 percent of the total drag force is frictional. Thus, the total increase in the drag coefficient due to roughness can be found. Furthermore, because power is directly proportional to resistance, the percent increase in effective horsepower, EHP, is the same as the total increase in the drag coefficient due to roughness. Finally, it is known that approximately 2.6 million dollars a year is spent on fuel for each DDG-51. By multiplying this amount by the total drag coefficient due to roughness, the amount of money spent in drag due to surface roughness per DDG can be calculated. These results are summarized in Table 2.

Table 2 – Results for Full Scale DDG-51

Surface	Roughness Height (μm)	% Increase in Frictional Drag	% Increase in EHP	Cost of fuel due to roughness in millions of dollars
New painted Ship Bottom Paint*	***130***	***6***	***4***	***0.1***
Fine Mesh	**380**	**60**	**39**	**1.0**
80 Grit Sandpaper	**690**	**51**	**33**	**0.9**
Medium Mesh	**1170**	**74**	**48**	**1.3**
Course Mesh	**1420**	**104**	**67**	**1.8**
40 Grit Sandpaper	**1800**	**78**	**50**	**1.3**
24 Grit Sandpaper	**3600**	**104**	**67**	**1.8**
Fouled Ship Bottom Paint*	***5000***	***178***	***116***	***3.0***

* - Schultz (2004)

The roughness penalty ranges from 0.9 million dollars for the smallest roughness tested to 1.8 million dollars for the largest roughness, which is a significant portion of the total amount of money spent for fuel. The ability to predict and subsequently reduce the drag due to surface roughness would result in significant fuel cost savings.

Even though ships will never be covered with a sandpaper or mesh surface, they still have hull roughness. This hull roughness typically ranges from a peak to trough roughness height of 150 microns for a newly painted ship to 1 centimeter for a fouled ship covered in barnacles (Schultz 2003). The sandpaper surfaces were measured in previous experiments using a laser

profilometer (Schultz, private communication). This allowed for the peak to trough roughness height to be found. The 80 grit, 40 grit, and 24 grit sandpaper surfaces had maximum peak to trough roughness heights of 690 microns, 1800 microns, and 3600 microns respectively. The mesh surfaces were measured using calipers. The wire diameter was measured along with the pitch, which is the distance of the space between wires. The maximum roughness height was taken to be twice the diameter of the wire since the wires overlap each other. The fine mesh, medium mesh, and coarse mesh had maximum peak to trough roughness heights of 380 microns, 1170, and 1420 respectively. The coarse, medium, and fine mesh pitch to diameter ratios were 4.5, 2.7, and 5.1 respectively. Although these surfaces are rougher than a brand new ship out of dry dock would have, they are still considerably smoother than a fouled ship and thus significant.

7. Experimental Procedures – Water tunnel Tests

All direct measurements of the mean velocity profile and turbulence were done using the re-circulating water tunnel in the Hydromechanics Laboratory at the United States Naval Academy. The test section of the water tunnel is 0.4 m x 0.4 m in cross section by 1.54 m long. The flow is produced by a four-bladed axial impeller which is powered by a 55 kW motor. This motor can vary the flow speed between 0 – 6.0 m/s. In this research project, the speed of the flow ranged from1.5 m/s to 3.75 m/s. The test plates (Figure 13) were 350 mm wide, 1.54 m long, and 12 mm thick. They were covered on one side with the roughness of interest which was held on using epoxy. The plates were then secured to a flat plate test fixture mounted horizontally in the bottom of the tunnel. A strip of 36-grit sandpaper was mounted on the forward 200 mm of the plate in order to trip the developing boundary layer to turbulent flow. Turbulence at the onset produces thicker boundary layers which allowed for easier measurements using the LDV downstream and fixes the location of transition giving more repeatable results. Measurements were made 1.35 m downstream of the leading edge of the plate. Previous studies in the same facility have shown that the flow adjusts back to the surface condition of the test plate well upstream of the measurement location. Because the system was closed, the growth of the boundary layer created a slight pressure favorable gradient on the test plate.

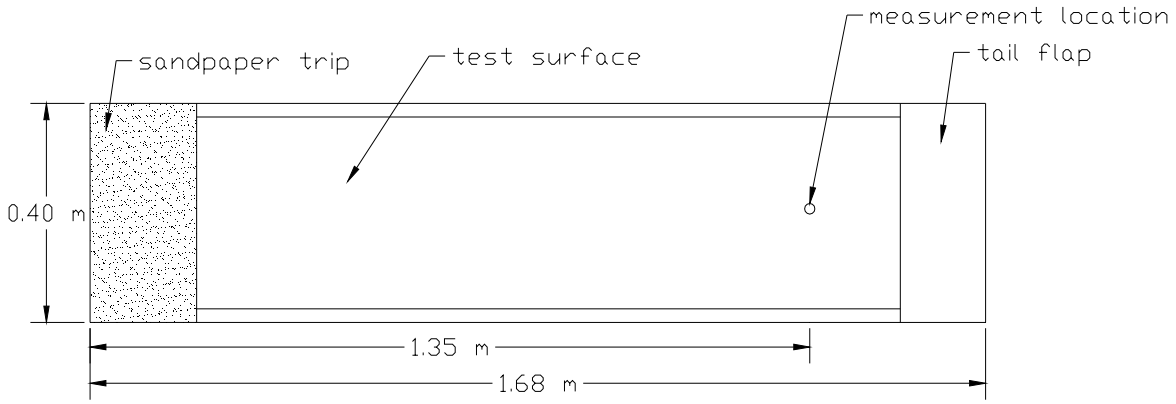

Figure 13 – Schematic of the flat plate test fixture

Velocity and turbulence measurements were made using a TSI IFA550 (TSI Inc., St. Paul, Minn., USA) two-component, fiber-optic laser Doppler velocimeter system. The LDV used a four-beam arrangement and was operated in backscatter mode. It was mounted on a three-axis traverse unit (Velmex Inc., Bloomfield, N.Y., USA). By crossing a laser light from two beams onto the moving fluid, the velocity of the fluid in one direction can be measured. At the crossing point the beams produce a fringe pattern due to constructive and destructive interference. As the particle passes through the fringes, light is scattered. The frequency of the scattered light (Doppler frequency) is a function of the particle velocity and the fringe spacing. An example of this can be seen in Figure 14 (Dantec Dynamics 2004). The scattered light is measured by the photo detector, which converts the light signal to a voltage. The voltage is then sent to a signal processor and on to a computer for high speed data acquisition and subsequent data reduction. Measured data is recorded at a rate of 100-500 Hz.

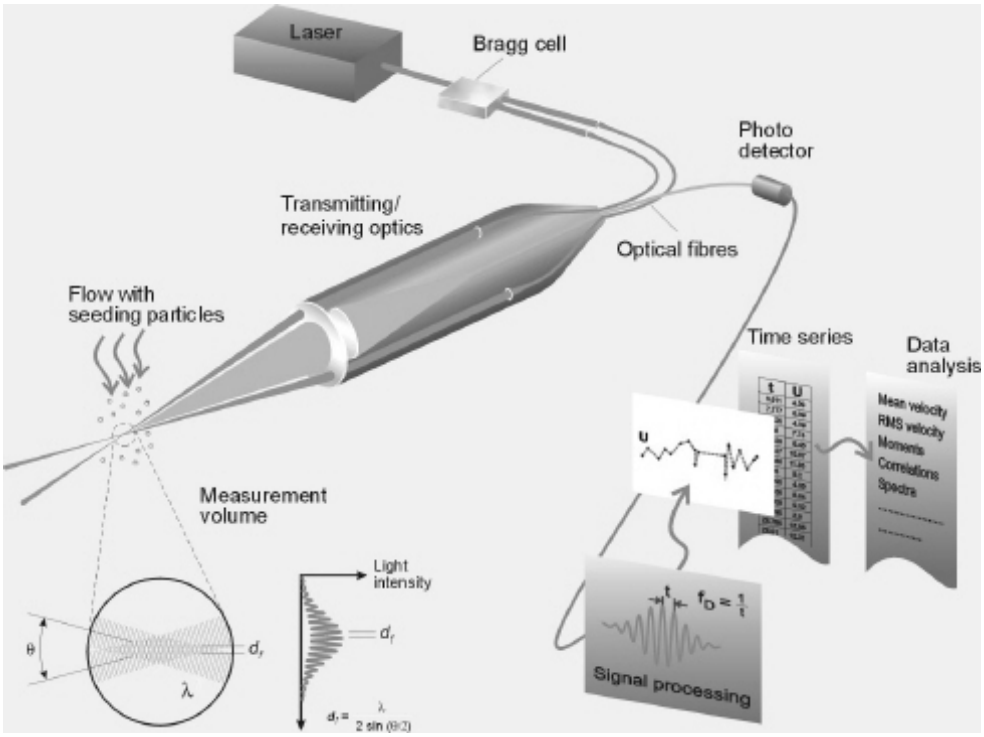

Figure 14 – Schematic of how a laser measures the velocity of a particle

For the current experiment, two components of velocity were recorded simultaneously. This requires two beam pairs that cross at the same location. Each beam pair uses a different wavelength of light. The signal from each pair is distinguished using filters. The flow was seeded with small glass spheres (10 μm diameter) which are neutrally buoyant. Velocities are obtained from the test plate surface to the edge of the boundary layer in the free stream using 40 logarithmically spaced points. This enables multiple data points to be taken close to the wall where the velocity gradient is large. A total of 20,000 random samples per location were obtained in order to ensure converged turbulence statistics. Since two components of velocity (4 beams) were obtained simultaneously, if Doppler bursts for the velocity measurements from each pair of beams did not fall within a 50 μm coincidence window, the sample was rejected.

8. Experimental Analysis of the Water Tunnel Results

Experiments were conducted on three test surfaces; the smooth plate, the 80 grit sandpaper, and the fine mesh surfaces. Due to the loss of equipment caused by Hurricane Isabel, experiments were not conducted on the other four surfaces. Both the smooth and sandpaper surfaces were tested using four different speeds; while, the fine mesh surface was only tested at one speed. This is shown in Table 3.

Table 3 – LDV Test Matrix

	Reynolds number based on downstream distance and freestream velocity			
Surface	1.4×10^6	3.4×10^6	4.1×10^6	4.7×10^6
Smooth	X	X	X	X
Mesh - fine	X	X	X	X
Mesh - medium	X	X	X	X
Mesh - coarse	X	X	X	X
Sandpaper - fine	X	X	X	X
Sandpaper - medium	X	X	X	X
Sandpaper - coarse	X	X	X	X

X = boundary layer profile

Uncertainty estimates based on multiple profiles on one surface

The turbulent boundary layer velocity profile for the highest Reynolds number can be seen in Figure 15. This profile of y vs. U contains the smooth surface, the 80 grit sandpaper surface, and the fine mesh surface. As expected, the smooth surface profile is fuller than the

rough surfaces since the smooth profile reaches the free stream velocity faster. This means that that there is a greater loss of momentum for the rough profiles, indicative of increased drag.

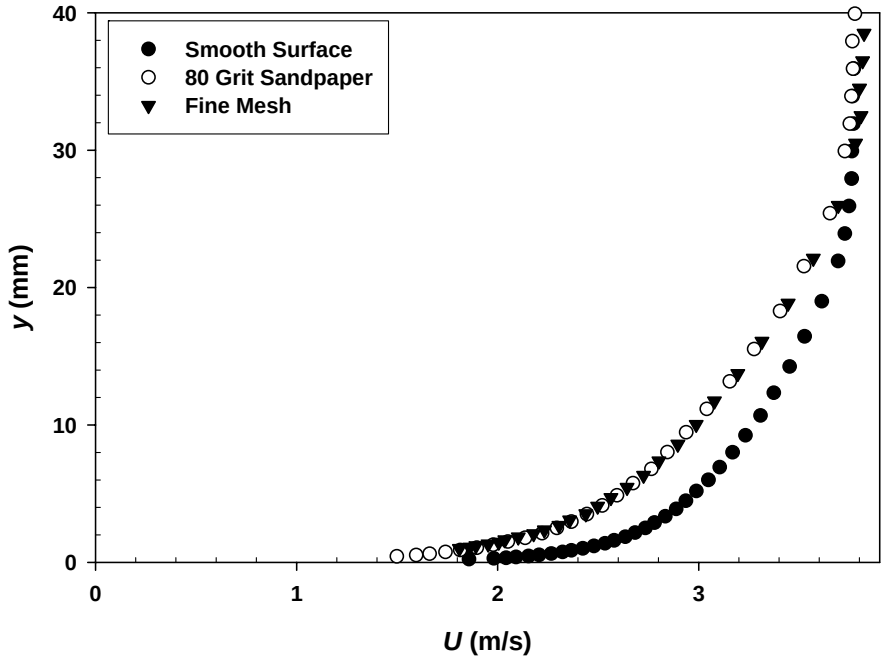

Figure 15 – Turbulent boundary layer profiles of all three surfaces tested

Measurements of boundary layer growth are the boundary layer thickness, δ, displacement thickness, δ^*, and the momentum thickness, θ. The boundary layer thickness, δ, is defined as the distance from the surface where the fluid velocity is 99.5% of the freestream velocity U_e. The displacement thickness is defined as the displacement of freestream fluid due to boundary layer growth on the surface. The momentum thickness is a measurement of the lost momentum due to the surface drag. These parameters serve as measures of the effect of surface conditions. The displacement thickness, δ^*, is defined by equation 11

$$\delta^* = \int_0^\infty \left(1 - \frac{U}{U_e}\right) dy \tag{11}$$

while momentum thickness, θ, is defined by equation 12.

$$\theta = \int_0^\infty \left(1 - \frac{U}{U_e}\right)\frac{U}{U_e}dy \tag{12}$$

Turbulent boundary layer results are often non-dimensionalized using the friction velocity, U_τ. This is considered an inner layer scaling as compared to the free stream velocity which is an outer layer scaling. In order to find the friction velocity, U/U_e is plotted versus $\ln(yU_e/\nu)$ where $y=y_{raw}+\varepsilon$ and ν is the kinematic viscosity. y_{raw} is the initial visual position of the laser at the wall, and ε is a correction that is added to y_{raw} in order to compensate for the fact that the laser was not initially positioned exactly at the wall at the start since the velocity at the wall is zero. Furthermore, with rough surfaces, the origin is not known because it could be at the top of the roughness peaks, the bottom of the roughness troughs, or somewhere in between (Perry and Li 1990). In order to induce the log law portion of the inner region to be linear in log normal coordinates, slight adjustments are made to ε and δ (Lewthwaite et al. 1985). This is checked by maximizing R^2, the coefficient of determination. An R^2 value can be calculated from this linear regression line which represents a portion of the total variance of the data points explained by the linear regression line. If R^2 equaled 1, all of the data points would lie on the linear regression line. However, since ε at the moment is still zero, the R^2 value will not be as high as it will once ε is correctly adjusted. Once the slope of the log law region is known, the skin friction coefficient, C_f, can be found, as shown in equation 13 (Lewthwaite et al. 1985).

$$C_f = 2\kappa^2 \left[\frac{\partial\left(\frac{U}{U_e}\right)}{\partial\left(\frac{yU_e}{\nu}\right)} \right]^2 \tag{13}$$

Figure 16 shows the skin friction coefficient versus momentum thickness Reynolds number for all surfaces tested. The smooth wall skin friction coefficient decreases with increasing momentum thickness Reynolds number, whereas C_f remains nearly constant for the 80 grit sandpaper. As expected, both rough surfaces have higher C_f values than the smooth wall. It is interesting to note that while the mesh roughness height was smaller than the 80 grit sandpaper, it produces higher skin friction. Therefore, skin friction is not solely dependent on roughness height.

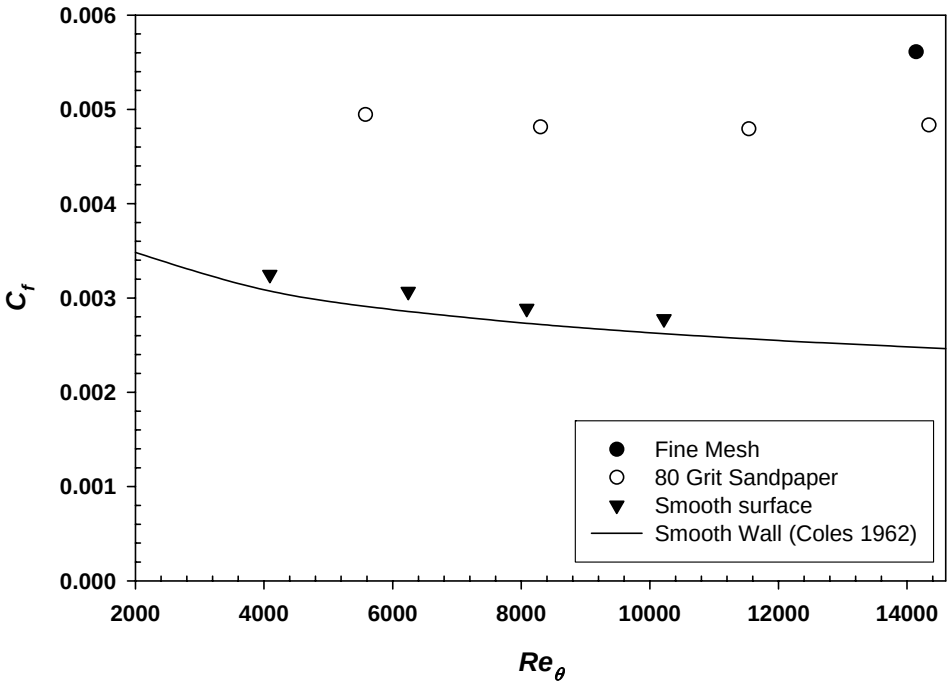

Figure 16 – C_f vs. Re_θ (overall uncertainty at 95% confidence is 4% for smooth surface and 7% for rough surfaces)

Now that C_f, is known, U_τ is calculated using equation 14

$$U_\tau = U_e\sqrt{\frac{C_f}{2}} \tag{14}$$

where U_e is the free stream velocity.

The roughness function, ΔU^+, is found directly from the measured velocity profile. Since the y-intercept for a smooth wall is 5.0, the roughness function of a rough wall can be determined by subtracting the known smooth wall intercept from the rough wall intercept (Lewthwaite et al. 1985). This can be seen in equation 15

$$U^+ = \frac{1}{\kappa}\ln y^+ + 5.0 - \Delta U^+ \tag{15}$$

which shows the mean velocity profile equation for a rough wall.

An example of the output of the spreadsheet used to perform all the steps necessary to find the roughness function can be seen in Table 4.

Table 4 – Example spreadsheet used to find the roughness function

downstream position (mm) 1350.00	**initial ε (mm)** 0.23	**step size (mm)** 0.01
lower limit constant 1.50	**ν (m^2/s)** 9.35E-07	**upper limit constant** 0.15
CALCULATED B.L. PARAMETERS		
U_e (m/s) 3.77	**δ (mm)** 26.40	**Log Law Slope** 2.44
c_f 0.0035	**δ* (mm)** 3.20	**Log Law Intercept** 5.00
u* (m/s) 0.14	**θ (mm)** 2.53	**Log Law R** 0.99995
roughness function, Δu+ 0.00	**y lower limit (mm)** 0.37	**y upper limit (mm)** 3.96

Table 5 summarizes all the results of the boundary layer thickness, displacement thickness, and momentum thickness. As expected, there is a significant increase in δ^* and θ for the rough surfaces.

Table 5 – Results from water tunnel tests (overall uncertainty of roughness functions at 95% confidence is 9%)

3.75 m/s				
	δ (mm)	δ* (mm)	θ (mm)	roughness function, ΔU^+
Smooth Surface	26.4	3.2	2.53	0.00
80 Grit Sandpaper	31.9	5.05	3.64	7.72
Fine Mesh	31.1	5.04	3.66	9.00
3.00 m/s				
	δ (mm)	δ* (mm)	θ (mm)	roughness function, ΔU^+
Smooth Surface	26.40	3.31	2.60	0.00
80 Grit Sandpaper	31.40	5.08	3.66	7.22
Fine Mesh	N/A	N/A	N/A	N/A
2.25 m/s				
	δ (mm)	δ* (mm)	θ (mm)	roughness function, ΔU^+
Smooth Surface	27.50	3.42	2.64	0.00
80 Grit Sandpaper	30.80	4.82	3.51	6.43
Fine Mesh	N/A	N/A	N/A	N/A
1.5 m/s				
	δ (mm)	δ* (mm)	θ (mm)	roughness function, ΔU^+
Smooth Surface	26.00	3.42	2.64	0.00
80 Grit Sandpaper	30.20	4.98	3.62	5.76
Fine Mesh	N/A	N/A	N/A	N/A

9. Discussion of Water Tunnel Results

The mean velocity profiles at the highest Reynolds number can be seen in Figure 17. This shows how the rough surface profiles of 80 grit sandpaper and fine mesh are shifted downward from the smooth profile; yet, they still maintain the same shape as the smooth profile. By using equation 16, the roughness function for the 80 grit sandpaper surface and the fine mesh surface are determined, as listed in Table 5. This figure indicates that the mesh and sandpaper surfaces tested display similar shifts from the log law even though the roughness type and size are different.

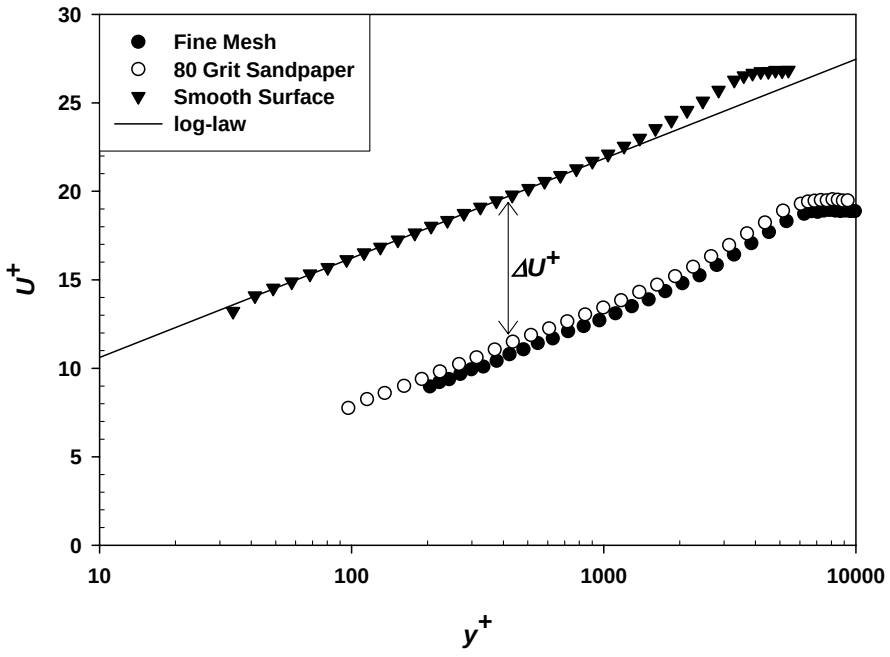

Figure 17 – Mean velocity profiles for all three surfaces

The velocity profile, $\frac{U_e - U}{U_\tau}$ versus $\frac{y}{\delta}$, is shown in Figure 18. This is called the velocity defect. Granville developed his similarity scaling on the assumption that the velocity defect profile would collapse both rough and smooth surfaces alike (Granville 1987). Furthermore, if the roughness functions of the rough surfaces measured directly do not equal those calculated from the tow tank tests, Granville's Similarity Theory does not apply. However, all three surfaces collapse on a single curve, indicating boundary layer similarity.

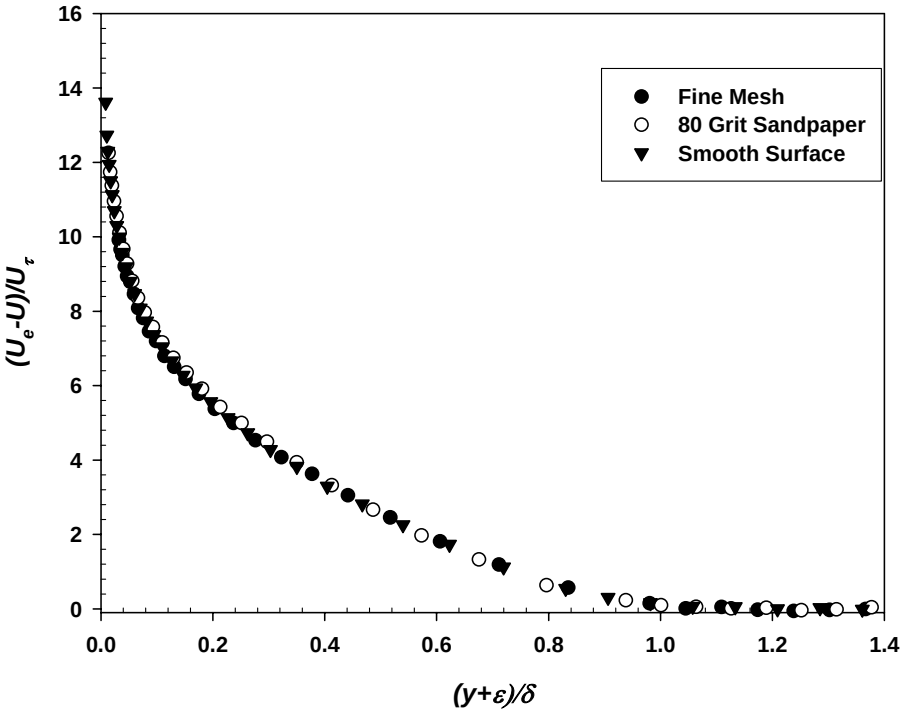

Figure 18 – Velocity defect profile

While numerous researchers have also observed this collapse including Clauser 1954, Hama 1954, Acharya et al. 1986, Granville 1987, Schultz 1998, Schultz & Myers 2003, a few studies, Krogstad et al. 1992 and Krogstad &Antonia 2001, noted differences in the defect profiles for the mesh type roughness.

Finally a graph comparing the roughness type to the roughness function can be made. This graph of ΔU^+ vs k^+ can be seen in Figure 19 for all of surfaces tested in both the Tow Tank tests and the LDV experiments. k^+ is called the roughness Reynolds number and represents the non-dimensional roughness height of a surface. By dividing k, the roughness length scale by the viscous length scale, the roughness Reynolds number is determined. The main difficulty is determining the proper roughness length scale to collapse results from disparate surfaces.

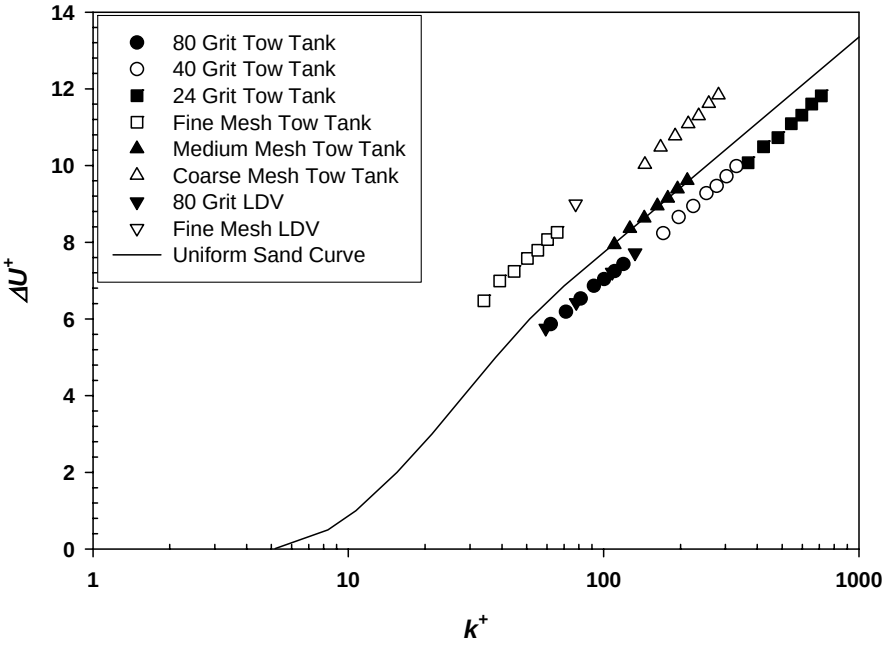

Figure 19 - ΔU^+ vs k^+ (overall uncertainty at 95% confidence is 9%)

The sandpaper surfaces all lie on the same line right below the uniform sand curve. The uniform sand curve was first created by Nikuradse who conducted experiments on the inside of circular pipes that had tightly packed, uniform sand grains glued to the walls (Schlichting 1955). Uniform sand is defined as mono-dispersed with uniform grain size; while, sandpaper is poly-dispersed with a wider range of grain sizes. Since the sandpaper surfaces all lie in a line with the same slope, a simple multiplication can be used to collapse the sandpaper surfaces to the uniform

sand curve. In order to get the proper values of k, the maximum peak to trough roughness height, R_t, was multiplied by a factor of 0.75, $k = 0.75\ R_t$ (Schultz and Flack 2003). Since R_t is a measure of the maximum sandpaper grain height, a multiplication factor must be added to account for the portion of the surface covered with a smaller grain size. This multiplication factor cannot be determined analytically or from a physical measurement of the surface, but must be determined experimentally. Figure 20 shows how multiplying R_t by 0.75 collapses the sandpaper surfaces onto the uniform sand curve.

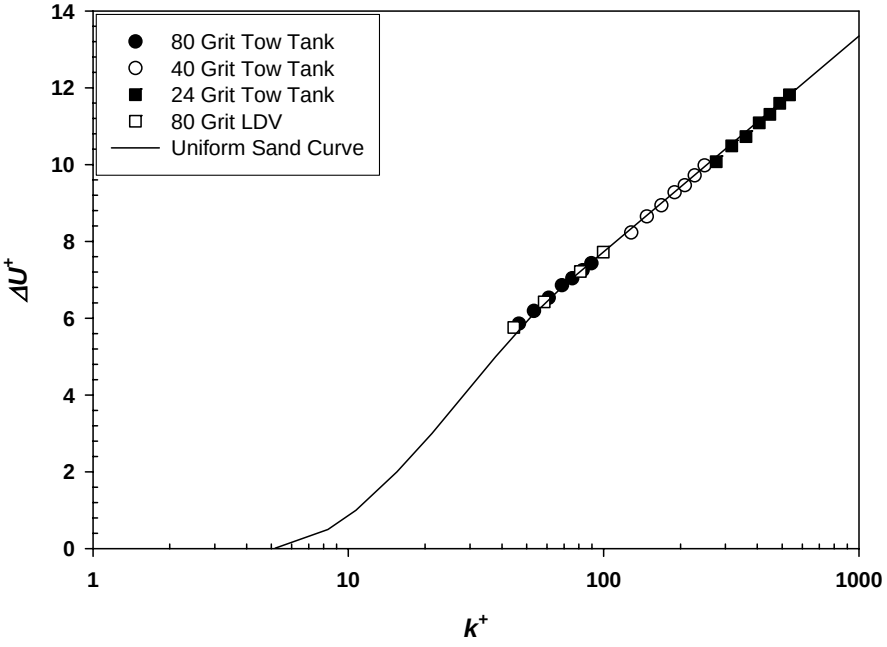

Figure 20 - ΔU^+ vs k^+ using the sandpaper scaling parameter, k=0.75R_t

Figure 20 also shows that the tow tank tests and the limited LDV measurements compare well. This can clearly be seen with the 80 grit sandpaper surface. The LDV test results lie right on top of the tow tank tests which is exactly what should be happening if similarity laws hold true. Whereas a simple multiplication factor can be used to collapse sandpaper surfaces; a different method must be used with the mesh surfaces.

Results for the fine mesh and course mesh surfaces do not lie on the uniform sand curve, however these surfaces follow a line with a similar slope. For the same value of k, these surfaces have a greater roughness function than a uniform sand surface. The differences observed on this plot can be explained by the pitch to diameter ratios and the peak to trough roughness height of the mesh surfaces. The coarse and fine mesh surfaces have similar pitch to diameter ratios, whereas the medium mesh surface has a significantly smaller ratio. It seems that the medium mesh surface affects the frictional drag in a similar manner as uniform sand surface, whereas the surfaces with larger pitch to diameter ratios do not. By performing a regression analysis of the data, an equation resulted by relating the roughness length scale, k, to the max peak to trough height, R_t, and the pitch to diameter ratio, p/d, as shown in equation 16.

$$k_s = R_t\left(0.45\frac{p}{d} - 0.20\right) \tag{16}$$

Because of the limited range of pitch to diameter ratios, the functional relationship should not be expected to describe all mesh surfaces. Furthermore, the graph which used this equation can be seen in Figure 21. Higher order polynomial fits did not yield significantly better results considering the limited number of mesh surfaces tested and the uncertainty in the measurement data.

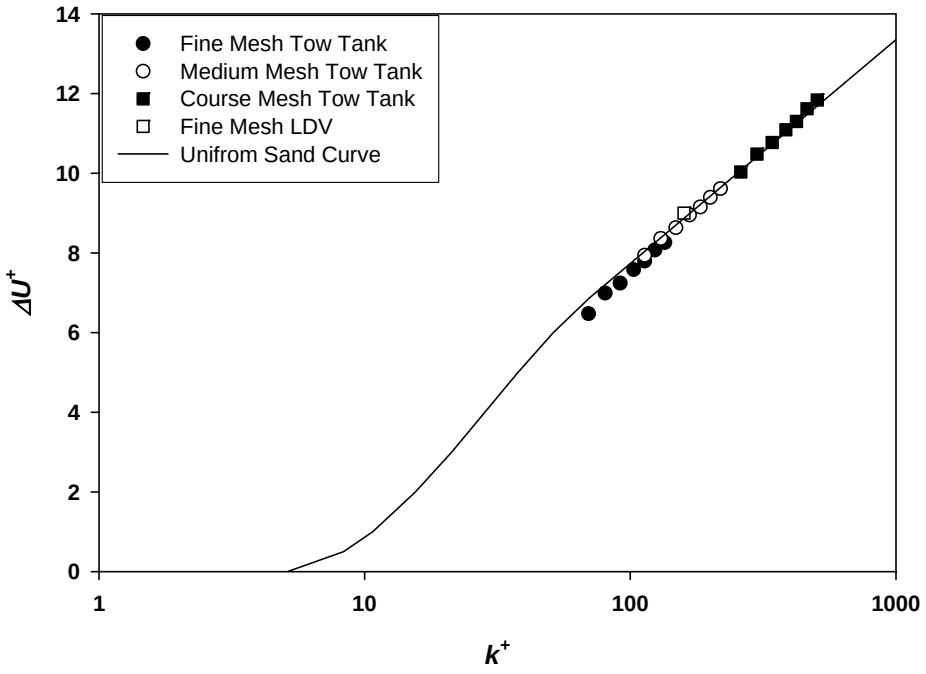

Figure 21 - ΔU^+ vs k^+ using equation 16

Recently there has been disagreement as to the effect of surface geometry on the flow in the outer portion of the turbulent boundary layer (Krogstad and Antonia 1999, Antonia and Krogstad 2001). A closer look at this project's turbulence results will now be made. There are three Reynolds stresses that need to be examined. The Reynolds stresses account for the additional stress due to the mixing caused by turbulent flow. The first one measures the Reynolds stress parallel to the flow and is also called the axial stress, u'^{2+}, the second measures the Reynolds stress normal to the flow and is also called wall-normal stress , v'^{2+}, and the third measures the Reynolds shear stress, $-u'v'^{+}$. The turbulence stresses, normalized by the frictional velocity, should all collapse for $y \geq 5k$ if the surface roughness does not affect the outer layer of the boundary layer. Figures 22, 23, and 24 show the Reynolds stresses start at a

maximum, and then decrease to a value of zero outside the boundary layer. This is due to the fact that the largest changes in the turbulence occur near the wall.

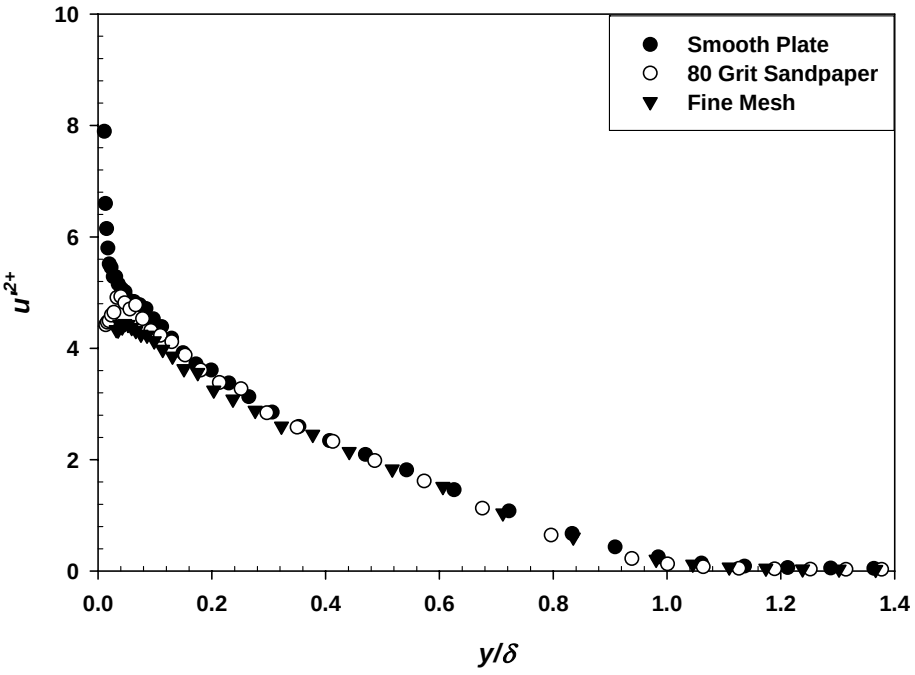

Figure 22 – Axial Reynolds stress

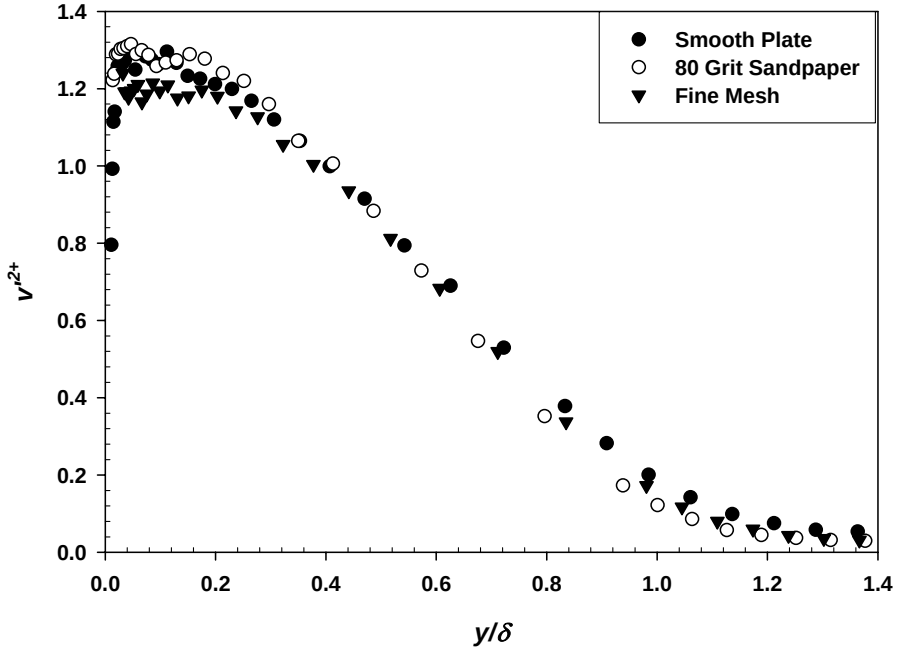

Figure 23 – Wall-normal Reynolds stress

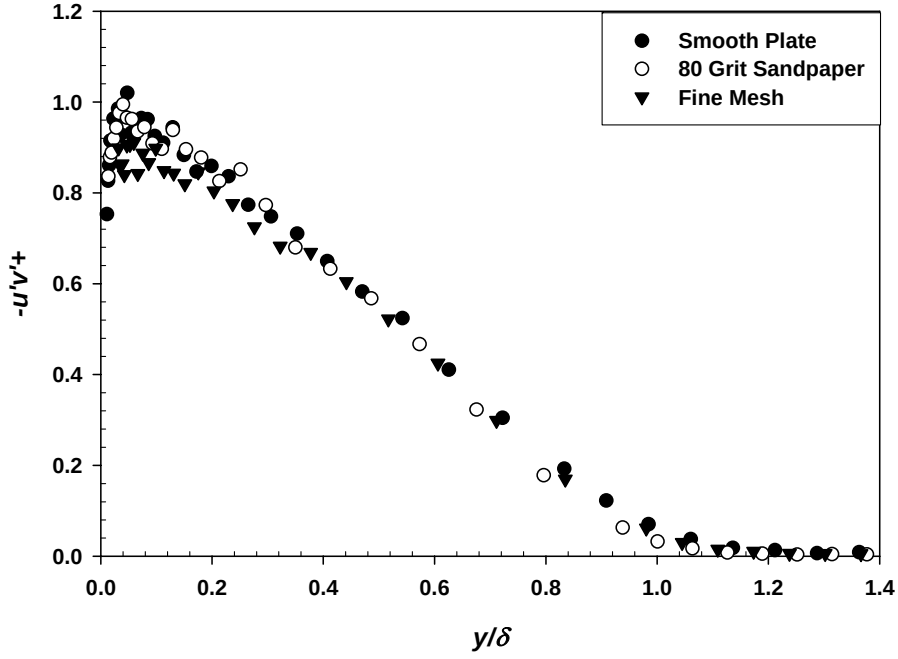

Figure 24 – Reynolds shear stress

Within the inner layer ($y/\delta < 0.2$), the roughness type is influencing the near surface turbulence. However, for $y/\delta > 0.2$, all figures show excellent collapse of the Reynolds stresses. This indicates that surface roughness does not affect the outer layer of the turbulent boundary layer regardless of the geometry of the roughness.

The importance of this result is that current models assume that the turbulence in the outer layer is independent of the wall roughness. These models, first published by Townsend in 1976 are called the Reynolds number similarity hypothesis. For the surfaces tested, Townsend's model holds true. It is interesting that the wall can change so much, from sandpaper to wire mesh, and the turbulence in the outer layer is not affected when scaled by the frictional velocity, U_τ. In addition, these results can help researchers who study turbulence in the outer layer because they can now confidently disregard surface roughness at high Reynolds numbers. Finally, a simple two layer empirical model based on smooth walls can now be modified to rough walls by including skin friction to the wall layer.

10. Conclusion

Seven different surfaces (one smooth, three sandpaper, and three mesh) were tested at various speeds in the 115 meter tow tank located in the Hydromechanics Laboratory at the United States Naval Academy, and the drag of each was measured. Using a laser Doppler velocimeter (LDV), velocity profiles for three surfaces (one smooth, one sandpaper, and one mesh) were also measured in a recirculating water tunnel. The project produced the following results:

- The roughness functions for the surfaces tested in the tow tank were calculated and the full scale frictional drag coefficient was predicted for a DDG-51 covered with a similar surface roughness. The results indicate a significant increase in fuel consumption with increasing roughness.
- The roughness functions for the velocity profiles measured with the LDV showed excellent agreement with the results from the tow tank test, indicating the validity of boundary layer similarity laws.
- Appropriate scaling parameters for the rough surfaces were developed. The sandpaper scaling parameter is directly proportional to the peak to trough roughness height, R_t, extending the results of previous research to a larger range of roughness height. A new scaling parameter for the mesh surfaces was developed which relates the pitch to diameter ratio as well as the peak to trough roughness height to the roughness function.
- The mean velocity profiles for the smooth and rough surfaces collapsed in defect coordinates indicating similarity in the outer region of the boundary layer. The Reynolds

stresses also showed excellent agreement in the outer layer, giving support to Townsend's boundary layer similarity hypothesis.

In the future, additional mesh surfaces with a wider variety of pitch to diameter ratios should be tested to enable the scaling parameter to be verified. Furthermore, rougher surfaces need to be tested in order to determine when roughness becomes too large and starts affecting the outer part of the turbulent boundary layer. At this point, current boundary layer models would fail and the similarity hypothesis would no longer be valid.

11. References

Alexandrou A. Principles of Fluid Mechanics. New Jersey: Prentice Hall, (2001).

Acharya M, Bornstein J, Escudier MP. "Turbulent Boundary Layers on Rough Surfaces." Experiments in Fluids 4:33-47 (1986).

Antonia RA, Krogstad P-A. "Turbulence Structure in Boundary Layers Over Different Types of Surface Roughness." Fluid Dynamics Research. 28: 139-157 (2001).

Bowen B, Davison N. "Resistance Increments Due to Hull Roughness Associated with Form Factor Extrapolation Methods." NPL ship Division Report TM 380 (1974).

Clauser FH. "Turbulent Boundary Layers in Adverse Pressure Gradients." Journal of Aeronautical Science 21:91-108 (1954).

Coles DE. "The Turbulent Boundary Layer in a Compressible Fluid." The Rand Corporation R-403-PR (1962).

Dantec LDV product page. Permission to use LDV picture given 13 February 2004. www.dantecdynamics.com

Franzini JB., Finnemore JE. Fluid Mechanics With Engineering Applications: Ninth edition. New York: McGraw-Hill, (1997).

Granville PS. "Three Indirect Methods for the Drag Characterization of Arbitrarily Rough Surfaces on Flat Plates." Journal of Ship Research 31: 70-77 (1987).

Grigson C. "The Full-Scale Viscous Drag of Actual Ship Surfaces and the Effect of Quality of Roughness on Predicted Power." Journal of Ship Research 31:189-206 (1987).

Grigson C. "Drag Losses of New Ships Caused by Hull Finish" Journal of Ship Research 36: 182-196 (1992).

Hama FR. "Boundary-layer Characteristics for Rough and Smooth Surfaces." Trans SNAME 62: 333-351 (1954).

Lewthwaite JC., Molland AF., and Thomas KW. "An Investigation into the Variation of Ship Skin Frictional Resistance with Fouling." Transactions Royal Institute of Naval Architects 127: 269-284 (1985).

Lewis EV. Principle of Naval Architecture: Second Revision. Jersey City: SNAME (1988).

Munson BR, Young DF, Okiishi TH. Fundamentals of Fluid Mechanics 4th Edition. New York: John Wiley and Sons, (2002).

Krogstad PA, Anotnia RA. "Surface Roughness Effects in turbulent Boundary Layers," Experiments in Fluids. 27: 450-460 (1999).

Perry AE, Li JD. "Experimental Support for the Attached-Eddy Hypothesis in Zero-Pressure-Gradient Turbulent Boundary Layers." Journal of Fluid Mechanics 218: 405-438 (1990).

Rotta JC. "Turbulent Boundary Layers in Incompressible Flow," Progress in Aeronautical Sciences, Vol. 2. eds A Ferri, D Kuchemann, LHG Sterne 1-220. Oxford: Pergamon Press, (1962).

Schlichting H. Boundary Layer Theory. New York: McGraw-Hill, (1955).

Schoenherr KE. "Resistances of Flat Surfaces Moving Trough a Fluid." Trans SNAME 40: 279-313 (1932).

Schultz MP. "The Effect of Biofilms on Turbulent Boundary Layer Structures." PhD Dissertation, Florida Institute of Technology (1998).

Schultz MP. Unpublished data (2003).

Schultz MP "Frictional Resistance of Antifouling Coating Systems." submitted to Journal of Fluids Engineering (2004).

Schultz MP, Flack KA. "Turbulent Boundary Layers Over Surfaces Smoothed by Sanding." Journal of Fluids Engineering (2003).

Schultz MP, Myers A. "Comparison of Three Roughness Function Determination Methods." Experiments in Fluids (2003).

Townsend AA. The Structure of Turbulent Shear Flow. Cambridge: Cambridge University Press, (1976).

Tupper E. Introduction to Naval Architecture: Third Edition. Oxford: Butterworth-Heinemann, (1996).